18th IFHTSE CONGRESS
International Federation for Heat Treatment and Surface Engineering
IFHTSE

SURFACE HARDENING OF A VC131 COLD WORK STEEL USING A FIBER LASER [1]

Flavia Aline Goia [2]
Milton Sergio Fernandes de Lima [3]

Abstract
Laser surface treatments represent some of most advanced and versatile processes for enhanced materials applications. Laser hardening is a technique to generate a hard wear-resistant surface microstructure in metals due to the rapid heating and cooling cycles imposed by a laser beam. This work intends to understand the influence of the laser variables on the hardness after laser hardening of a VC131 steel. A fiber laser, which is a new source available for industrial applications, has been used. The overall absorptivity measured was approximately 37% and the laser treatment produced two different zones: remelted and heat-affected. The surface layer was remelted and composed by martensite and retained austenite. The region next to the free surface is composed by primary austenite dendrites with martensite plates with hardness between 400 and 500 HV. The region called heat-affect zone is composed by martensite, retained austenite and carbides and has hardness up to 800 HV. The case depth in laser treated samples was between 1 and 2 mm.
Key words: Surface hardening; Laser hardening; Steel hardening; Laser processing.

[1] *Technical contribution to the 18th IFHTSE Congress - International Federation for Heat Treatment and Surface Engineering, 2010 July 26-30th, Rio de Janeiro, RJ, Brazil.*
[2] *M.Sc. student in Instituto Tecnologico de Aeronáutica (ITA), Sao Jose dos Campos, SP, Brazil.*
[3] *Researcher in Instituto de Estudos Avançados (IEAv) and professor in Instituto Tecnologico de Aeronáutica (ITA), Sao Jose dos Campos, SP, Brazil.*

1 INTRODUCTION

Laser surface hardening is a method of producing martensite on selected regions of steel components. Usually a continuous wavelength laser is scanned over the item to heat the surface up to the austenite range (approximately 1000°C in most steels). Since the substrate acts as an efficient heat sink, the material is quickly cooled down to a temperature below Ms (martensite start temperature[1]) behind the moving laser beam. The resulting microstructure is composed of fine martensite, which improves both mechanical and chemical surface properties, but maintains unchanged material bulk properties, like ductility and toughness.

There are some differences between laser and conventional heat sources like flame and induction for surface hardening. The laser process is quite fast and could produce metastable phases. Also, it induces elevated temperature gradients near to the exposed surface, leading to an austenitizing temperature that is higher than the usual processes to allow thermal penetration. In some cases, the temperature is so high that some remelting occurs and the region near to the surface is composed by a resolidified layer.[2] Some remelting is particularly attempted when multiphase steels or cast irons are treated,[3] generating a more homogeneous layer.

Because of wide availability, both CO_2 and Nd:YAG lasers have been used to produce hardened surfaces on steels.[4-6] When using CO_2 lasers, coatings are usually needed in order to increase the laser-matter surface absorptivity. One popular method to achieve this is by spraying the surface with colloidal graphite, which can be easily removed after the treatment. Solid-state lasers, such as Nd:YAG or diode lasers, with shorter wavelengths, produce better laser-matter coupling, and so an absorptive coating might not be necessary. High-power diode lasers are very popular for surface hardening due to the high absorptivity of metals and the typical rectangular beam shape, approximately a top hat in both directions, which allows large areas to be treated. Kennedy et al.[7] reviewed the literature on the use of high-power diode lasers for surface hardening.

Another type of laser source was recently appeared as a competitor of Nd:YAG, CO_2 and diode lasers for materials processing: the fiber laser. Differently from the other sources, the fiber is both the gain and the delivery media for laser radiation, without moving parts or mirrors to be aligned. The fiber laser is basically plug-and-play industrial equipment absent of maintenance for more than 20.000 hours. Automation is easy since the optical fiber is delivery directly from the laser cavity to the processing head. The same laser source could be used to cut, weld or heat-treat a number of materials. Similarly to the diode laser, the focal plane could be fixed at the image of the fiber, generating a top-hat energy distribution.

Lima et al.[2] studied the effect of fiber laser hardening in an AISI 1040 steel automotive shaft. These authors verified a case depth up to 0.3 mm using a 900 W laser beam scanned at 2 mm/s over the shaft turning at 120 RPM. The maximum hardness obtained was 800 HV compared to 300 HV of the base steel.

The aim of the present work is to develop a systematic approach for laser hardening of the VC 131 steel using a fiber laser and to investigate the obtained microstructure. The VC 131 class is a cold work steel presenting a good balance of hardness, toughness, dimensional stability and wear resistance and it is used in various applications like industrial knives, rulers and cutting die. A suitable method to enhance the surface hardness without affecting toughness and ductility of the bulk metal will be of interest for many industries.

2 MATERIALS AND METHODS

The steel used here is a VC 131 grade produce by Villares Metals Co.,[8] similar to standards DIN X 210, CrW 12, Wnr 1.2436, AISI D6 and ABNT D6. The chemical composition is given in Table 1.

Table 1. Chemical composition of the VC 131 (balance = Fe)

C	Cr	W	V
2,10	11,5	0,70	0,15

The as-cast microstructure is composed by ferrite, carbides (specially Cr_7C_3), pearlite and bainite. The material is furnished on the annealed condition with a hardness of 240 HV. For each experiment, a 13 mm thick slice of a 70 mm diameter bar was machined and grinded with to 600 SiC paper.

A 2 kW continuous wave fiber laser produced by IPG Co. was used here. The laser radiation is generated in 50 μm diameter fiber doped with ytterbium. The doped fiber is connected to a process fiber with 100 μm diameter and 10 m long, which is then connected to an Optoskand processing head. The focal length was 157 mm with a minimum spot diameter of 100 μm, but the actual radius ω(Z) depends on the position of sample surface in respect to the focal plane, as presented in Equation 1.

$$\omega(Z) = \omega_0 \left[1 + \left(\frac{M^2 \lambda . Z}{\pi . \omega_0^{\,2}} \right)^2 \right]^{1/2} \qquad \text{Equation 1}$$

Where: Z is the distance from focal plane, ω_0 is the minimum beam radius, M^2 is the beam quality factor (9) and λ is the laser wavelength. Here, Z is a variable, ω_0 = 50 μm, M^2 = 12 and λ = 1,080 μm. The seller furnished the value of M^2.

Pure argon gas at 30 l/min flow rate had been used to protect the surface against oxidation. The protection gas was delivered trough a rounded copper tube of 3 mm internal diameter directly over the irradiated area.

The samples moving is realized by a CNC table. The table moves at constant velocity from 1 to 160 mm/s and could be programmed to any direction in an area of 430 x 508 mm^2. The Z-axis is also computer controlled with a 1 μm step resolution and is used to change the focal distance Z (Equation 1). In order to process an entire surface, the laser beam moved in squared zigzag with partial superposition between the tracks. It is also possible to pulse the laser beam in durations from 1 ms to continuous wave. The pulsed mode was used here to investigate the laser-material interaction.

The absorptivity of the laser beam during processing is measured as proposed elsewhere[10] using calorimetry. The absorbed energy was measured by recording the temperature evolution over time from two thermocouples fixed on the opposite face of the samples. An alumina tissue was used to isolate the sample from surroundings, being only the upper surface exposed to the laser. Considering the sample as a calorimeter, the absorptivity could be estimated by Equation 2.

$$\beta = \frac{m.C_p(T_{max} - T_a)}{P.t_i} \qquad \text{Equation 2}$$

Where β is the average absorptivity in the sample, m is the mass, C_p is the specific heat, T_{max} is the maximum temperature, T_a is the ambient temperature, P is

the laser power and t_i is the interaction time. Here, m = 352,0 g, C_p = 0,460 $J.g^{-1}.°C^{-1}$[11] and t_i is the time where the laser is on over the piece.

Microstructural analyses were carried out using Optical Microscopy (OM), Microhardness Testing (HV) and X-ray Diffraction (XRD). The optical microscope is a reflected light Reichert Polyvar 2 equipped with acquisition system and image processing software. The microhardness tester is a Future-tech FM 700 equipment using a Vickers pyramid and loads from 5 to 500 gf. Here, the applied load was 200 gf and the application time was 9 s. X-ray diffraction equipment is a Isodebyefley 1001 (Seisert) using the Cukα radiation. The angle range was between 30 and 110° (2θ) and the crystalline phases were analyzed using a JCPDS (Joint Committee of Powder Diffraction Standards) library.[12]

3 RESULTS AND DISCUSSION

For the first set of experiments, the sample surface was divided in 23 different regions and each region received a shot with different laser power P and focal distance Z. The aim is to investigate the effect of different intensities on hardening and melting behavior. The pulse time length was fixed at 1 second. Table 2 shows the consolidated results together with the calculated intensity (I), using the beam diameter give in Equation 1, the melting occurrence and the hardness in the resolidified (MZ) and heat-affect zones (HAZ). For comparison, the base material hardness was 240±20 HV.

Table 2. Single-shot laser parameters and results

Shot	P (W)	Z (mm)	I (W/cm^2)	Melting (Y/N)	Hardness (HV)	
					MZ	HAZ
1	100	+50	191	N	*	*
2	100	+30	529	N	*	*
3	300	+50	572	N	*	*
4	300	+50	572	N	*	*
5	200	+40	595	N	*	*
6	400	+50	762	N	*	*
7	300	+40	893	N	*	*
8	500	+50	953	N	*	*
9	200	+30	1058	N	*	*
10	600	+50	1143	Y	*	603±30
11	400	+40	1191	Y	*	590±60
12	700	+50	1334	Y	510±40	600±40
13	100	+18	1469	N	*	*
14	500	+40	1488	Y	620±90	780±50
15	800	+50	1524	Y	550±20	550±40
16	300	+30	1587	Y	660±40	820±90
17	900	+50	1715	Y	520±10	560±50
18	400	+30	2116	Y	570±30	530±20
19	500	+30	2645	Y	550±20	430±10
20	200	+18	2937	Y	580±20	560±40
21	300	+18	4406	Y	520±20	470±60
22	400	+18	5875	Y	550±30	640±70
23	500	+18	7343	Y	530±10	520±20

** Any interaction visible; hardness similar to the base material or too tiny to be measured.*

As can be seen in Table 2, laser intensities below about 1 kW/cm^2 did not produce measurable hardening effect. Another experimental limitation is observed for the 100W power shots, e.g. shot # 13, were the laser cavity could not work appropriately and the emission is not actually observed.

The laser treated steel had an average hardness between 510 and 620 HV for the resolidified zone. This represents about two times the hardness of the base material. The HAZ presented a hardness range much wider than MZ, with an average value of 590 HV. The shots numbered 14 and 16 presented hardness values well above the average in the HAZ, attained up to 3.4 times the base material HV. This indicates two important facts: a) maximum hardening effect is obtained around 1.5 kW/cm^2 and b) under these intensity levels, and using the current laser configuration, melting occurs during processing. Therefore, the current laser processing could be better defined as laser hardening through melting, as previously cited by Chiang and Chen.[13]

Since the differences on hardening between MZ and HAZ values deserve further analyses, the HV profile of a cross section of the shot 14 was analyzed. A graphic representation of the cross-sectional area together with the hardness measurements is presented in Figure 1. The measurements started 25 μm below the upper surface and the step from the center was 25 μm also. As could be seen in Figure 1, the average hardness of 620 HV in the MZ increased near to the interface MZ/HAZ. This region by the MZ/HAZ is heated near to the liquidus temperature and thus presents a high diffusivity and a high austenitization time compared to other regions, which leads to more martensite being formed. This could be also seen when analyzing the sample in depth, as presented in Figure 2, where the marks represent the HV pyramid indentation. The primary Cr_7C_3 carbides remained during heating in the HAZ, but were dissolved in the MZ (white layer). Since the Cr is dissolved in the MZ, the Ms temperature substantially decreases[14] which greatly reduces the probability of martensite transformation even at high cooling rates. On the other hand, the HAZ next to the melted zone (arrow in Figure 2) undergoes high cooling rates and limited Cr-dissolution; therefore comparatively more martensite is formed during cooling. This is the reason the MZ is softer than HAZ.

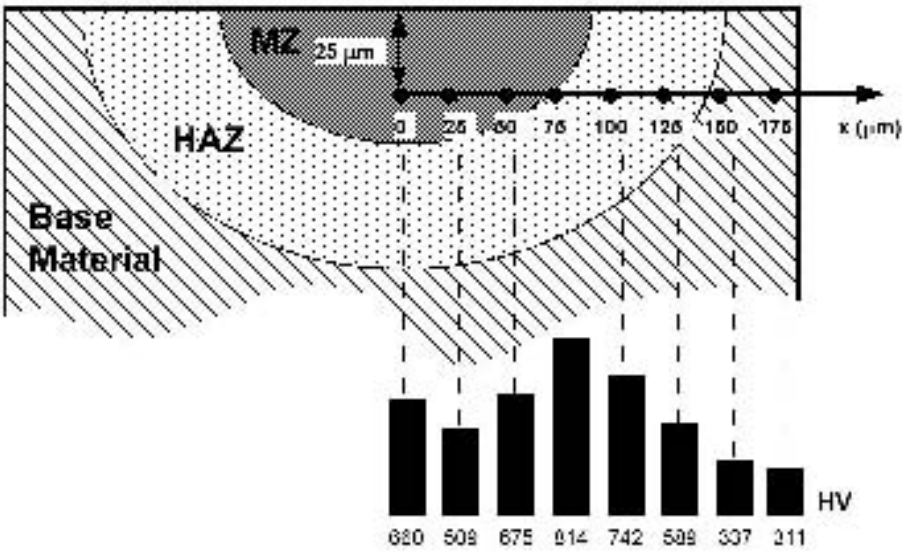

Figure 1. Schematic picture of a cross section of shot 14 and the HV profile.

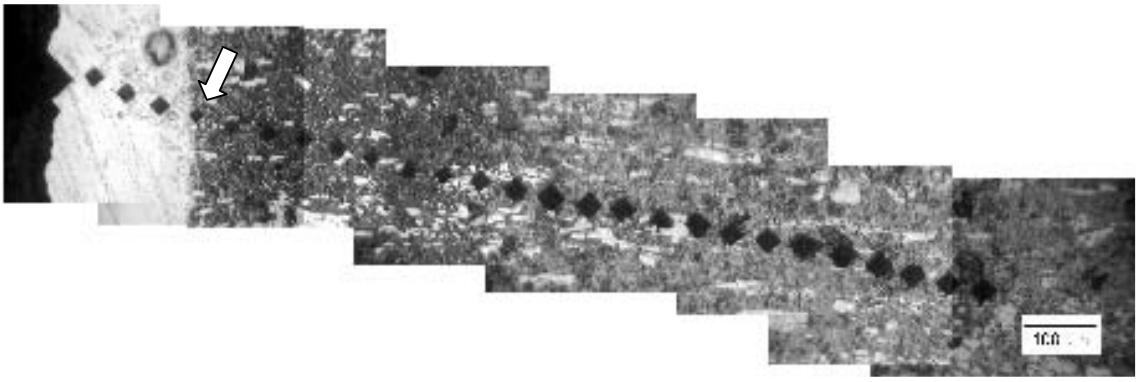

Figure 2. A sequence of Vickers indentations made on the cross section of shot 14.

These laser shot experiments assisted to decide what are the best conditions for line scan analyses. These conditions are:

- Line A – similar to shot 16, where P=300W, Z=30mm, spot diameter = 2ω(Z) = 4.9 mm. This shot presented the highest value of hardness in the HAZ;
- Line B – similar to shot 14, where P=500W, Z=40mm, spot diameter = 2ω(Z) = 6.5 mm. It also presented high hardness values.; and
- Line C – similar to shot 10, where P=600W, Z=50mm, spot diameter = 2ω(Z) = 8.2 mm. This shot represents the limiting intensity value for hardening, but could be interesting for study because more interaction is observed during line scanning.

The linear velocity for each Line must be the spot diameter at surface divided by the exposure time. Since every laser shot was release during 1 second, the linear laser speeds were 4.9, 6.5 and 8.2 mm/s for lines A, B and C, respectively.

One sample was then laser treated using these three experimental conditions A, B and C, repeated once each. Figure 3 shows the surface aspect of the laser treated sample, showing six laser tracks being (‘) meaning a repetition of the previous condition. During the laser treatments, the temperature was recorded using two thermocouples placed at the opposite face of that shown in Figure 3. Table 3 presents the results of the calorimetric study, where: l is the length of the laser line on the sample, Δt is the duration of the laser at every treatment, ΔT is the temperature rise at the end of treatment, β is the laser-steel absorptivity and $\Delta\beta$ is the standard deviation. As can be seen, the average laser absorptivity on the steel was about 37%, i.e. roughly one-third of the laser power is effectively absorbed by the surface. This value is higher than those observed from CO_2 laser, about 10%, and similar to the observed for diode lasers.[15]

A hardness profile at the surface and perpendicular to laser tracks where then realized for the sample of Figure 3, and the results are presented in Figure 4. The maximum attained hardness were approximately 600, 800 and 600 HV, for lines A, B and C, respectively. These results were similar to those obtained in single shots (Table 2), with an improvement of hardenability under conditions of Line B. These conditions seem to be an optimized set between a high melting volume (Line A) and an insufficient heat transfer (Line C).

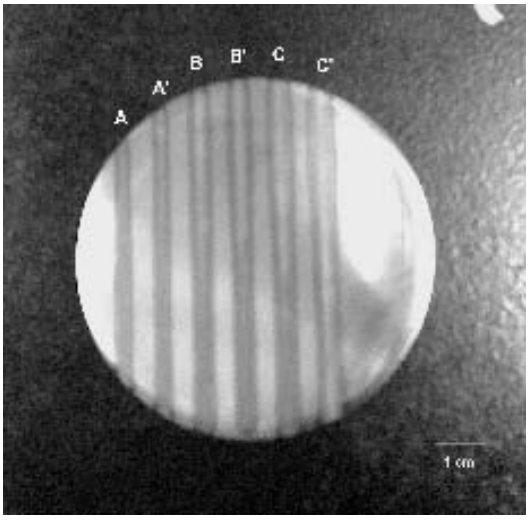

Figure 3. Laser treated sample with 3 types of different linear treatments.

Table 3. Results of thermal analyses

Line	P (W)	V (mm/s)	l (mm)	Δt (s)	ΔT (s)	β	Δβ	β (%)
A	300	4.9	60.0	12.25	7.5	0.33	0.03	33
B	500	6.5	69.0	10.61	12.2	0.37	0.02	37
C	600	8.2	64.4	7.86	11.9	0.41	0.03	41

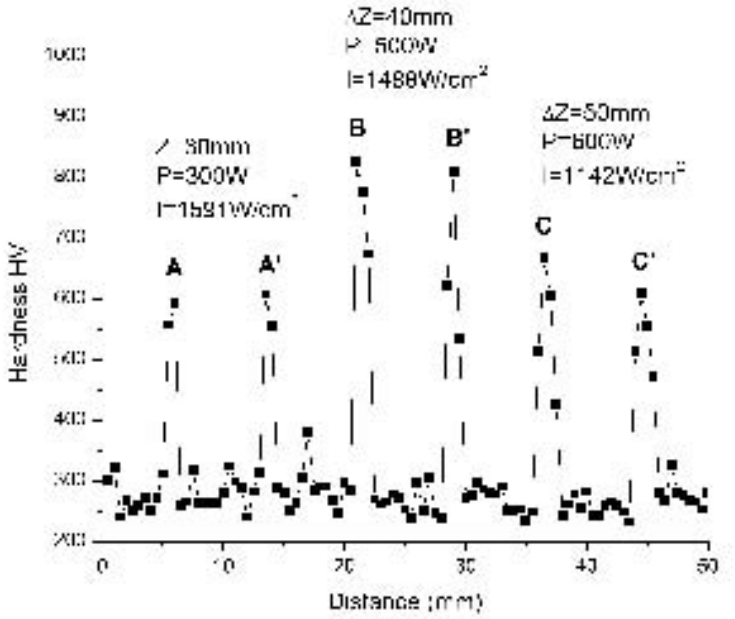

Figure 4. Hardness profile of a transversal line in the sample shown in Fig. 3.

Figure 5 presents the hardness profile in depth after a transversal cut and polishing of the sample. The conditions Line A and Line C produced almost the same case depth, with a hardened zone of about 0.1 mm. On the other hand, the condition Line B presents a case depth of about 0.3 mm. The Line B condition seems to allow improved thermal penetration with little melting.

From the above analyses, it could be reasoned that the condition Line B was the best in terms of hardness and case depth values. Therefore, the experimental conditions of Line B had been retained for the entire surface preparation.

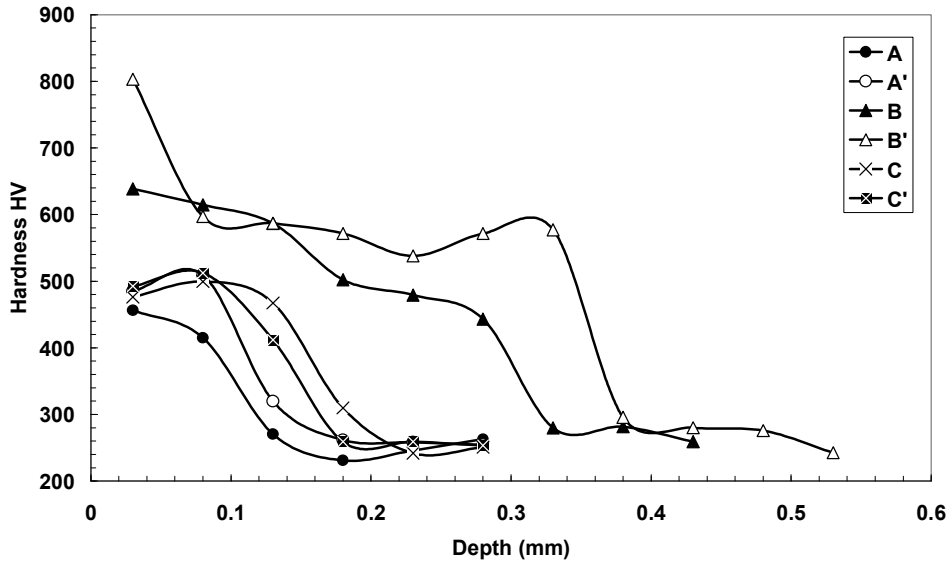

Figure 5. Hardness profile in depth of the sample.

The surface treatments were carried out using different tracks superposition, as presented in Figure 6. In the figure, it is presented a schematic representation of the hardened zone and how the calculations were made. For each condition S1, S2 and S3 a given superposition was designed, considering the total length LT was 2.74 mm. For the present case, the superposed length is LS and Y represents the distance between the HAZ boarder and the center of previous track.

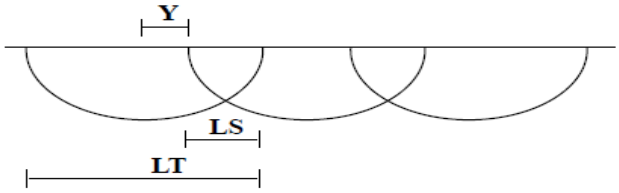

$$LS\% = 100 - \left(\frac{LT - LS}{LT} \times 100 \right)$$

Measurements of LS and Y			
Condition	LS (%)	LS (mm)	Y (mm)
S1	50	1,37	1,37
S2	80	2,19	0,55
S3	30	0,82	1,92

Figure 6. Experimental measurements of the hardened layer and the superposition length.

The microstructural results were presented in Figure 7. The white zone represents the remelted layer is composed by primary austenitic dendrites that are partially converted to martensite. A close examination shown that carbides, supposed

Cr_7C_3, were verified in the interdendritic region. The heat affect zone was observed as the darkened region just below the remelted layer. The extensions of each zone and the linked average hardnesses were:

- **S1**: MZ = 0.3 mm (430 HV); HAZ = 0.8 mm (490 HV);
- **S2**: MZ = 0.8 mm (450 HV); HAZ = 1.0 mm (610 HV); and
- **S3**: MZ = 0.2 mm (410 HV); HAZ = 0.5 mm (520 HV).

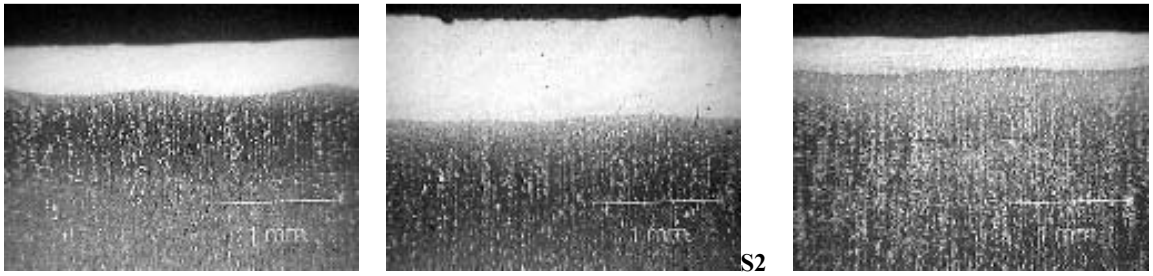

Figure 7. Cross-sectional micrographs of the surfaces after laser treatment.

The superposition greatly influenced the case depth and the average hardness due to sum of line scan contributions. The average hardness of the melted zones (MZ) decreased due to the tempering effect that decreases the amount of martensite. On the other hand, the HAZ are less affect by consecutive heating and presents already a high hardness value. The condition S2 presented the higher HV value due to the carbide precipitation in the Cr-rich remelted layer.

The surfaces were then studied by X-ray diffraction, as presented in Figure 8. The samples were analyzed by the JCPDS standards and the associated files were displayed in the right-upper corner in Figure 8. The as received, unlasered condition, is mainly ferritic and the carbides peaks are not resolved. The lasered conditions S1, S2 and S3 show peaks of martensite (α') and austenite (γ). The ratios between the intensity of peak 101 of martensite and peak 200 of austenite were almost the same in all specimens, being approximately 2.2. Therefore, it could be concluded that the percentage of austenite and martensite is the same regardless the superposition.

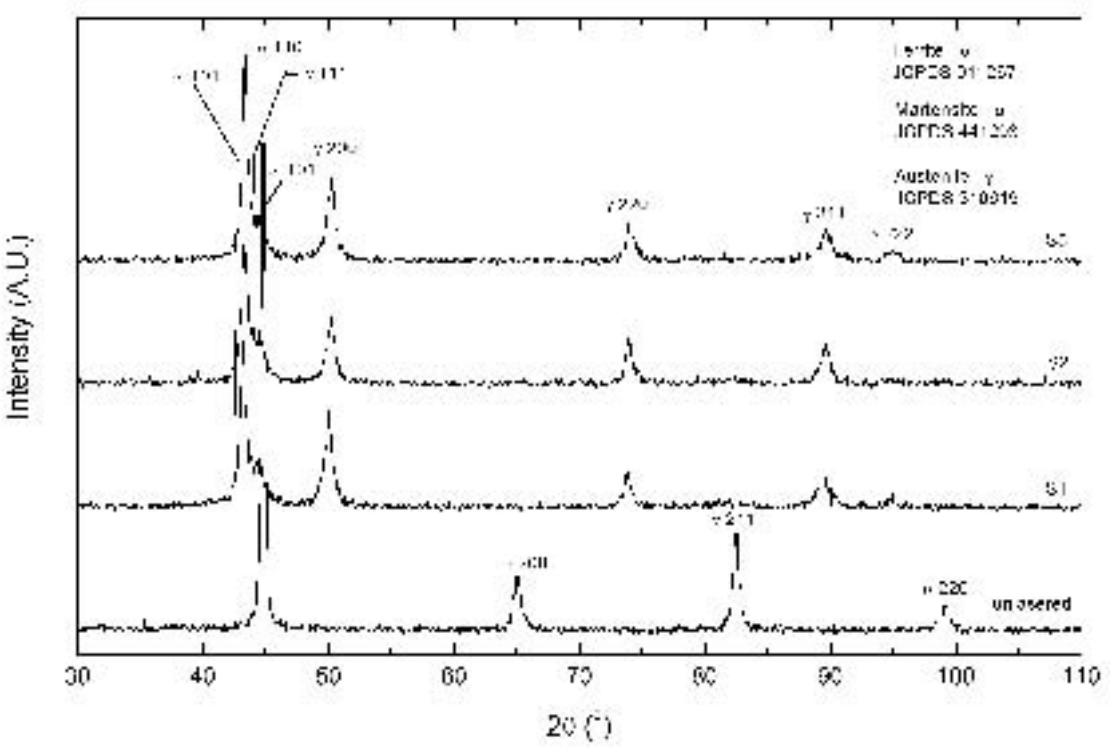

Figure 8. X-ray diffraction analyses of the unlasered and laser processed surfaces.

4 CONCLUSIONS

After analyzing the results, the following conclusions could be draw:

The proposed methodology, based on a stepwise understanding of the laser-matter interaction, from single shot to entire surface treatment, has the advantage to help reach the sought goal. This is particularly true for laser materials processing where many different variables could interact.

Different laser parameters produced different results in terms of case depth and hardness for the VC 131 steel. The best results was obtained when the focalization was fixed at Z=40 mm, the laser power set at 500 W, the scanning speed fixed at 6.5 mm/s and the superposition between laser tracks attained 80%. Under these conditions, the VC 131 hardened zone, composed by both resolidified and solid-state regions, attained 1.8 mm in depth. The resolidified surface is mainly composed by martensite and retained austenite and the heat-affected zone is composed by martensite and undissolved carbides.

Under the current laser configuration, hardening is only obtained by allowing some surface melting. This surface melting helps improve laser absorptivity on the piece which is about 1/3 of the incident intensity.

Acknowledgements

The authors thank Financiadora de Estudos e Projetos (FINEP) for funding the laser and Mr Denys Flores from Mahle-Metal Leve Co. for expert advises. Thanks also are due to Dr Paulo Suzuki of Escola de Engenharia de Lorena/Universidade de São Paulo for X-ray diffractometry.

REFERENCES

1 PORTER, D.A.; EASTERLING, K.E. Phase Transformations in Metals and Alloys, 2nd. edition, CRC Press: New York, p. 382-430, 1992.
2 LIMA, M.S.F.; GOIA, F.A.; RIVA, R. Laser surface remelting and hardening of an automotive shaft using a high-power fiber laser. *Materials Research*, v.10, n.4, p. 461-467, 2007.
3 LIMA, M.S.F. Uma contribuição ao estudo da microestrutura dos ferros fundidos refundidos superficialmente por laser. Thesis (PhD). Escola Politécnica da Universidade de São Paulo, 1997, 167p.
4 BACH, J.; DAMASCHECK, R.; GEISSLER, E.; BERGMANN, H.W. Laser transformation hardening of different steels. In: H.W. Bergmann, R. Kupfer, eds. *Proceedings of the 3rd European Conference on Laser Treatment of Materials (ECLAT´90)*.Coburg: Sprechsaal Publising Group. p. 265-282, 1990.
5 HINO, M.; HIRAMATSU, M.; AKIYAMA, K.; KAWASAKI, H.; TSUJIKAWA, M.; KAWAMOTO, M. Surface Hardening of Carbon Steel Using High Powered YAG Laser, *Materials Manufacturing Processes*, v. 12, p. 37-46, 1997.
6 PENG, R.L.; ERICSSON, T. Residual stress distributions in laser transformation hardened steels, *Scandinavian Journal of Metallurgy*, v. 27, p. 223-232, 1998.
7 KENNEDY, E.; BYRNE, G.; COLLINS, D.N. A review of the use of high power diode lasers in surface hardening, *Journal of Materials Processing Technology*, v. 155–156, p. 1855–1860, 2004.
8 VILLARES METALS. Aços para trabalho a frio VC131. Folheto informativo, 2p. 2006.
9 Melles Griot Co. Gaussian Beam Optics. Technical Manual, p. 2.1 - 2.14, 2005.
10 LIMA, M. S. F., WAGNIÈRE, J. D. Determinação da absorção do feixe laser em ensaios de refusão em regime contínuo. *Revista de Metalurgia*, v. 32, p.131 - 134, 1998.
11 Automation Creations, Inc. Material Property Data: Specific Heat on Steels. Avaliable in: http://www.matweb.com/. Access 10 June 2009.
12 JCPDS, Program for Powder Diffraction Files, v.2.3, International Center for Diffraction Data, Pennsylvania, USA, 2002.
13 CHIANG, K.-A.; CHEN, Y.-C. Laser surface hardening of H13 steel in the melt case, *Materials Letters*, v. 59, p. 1919-1923, 2005.
14 ROWLAND, E.S.; LYLE S.R. The Application of Ms Points to Case Depth Measurement, *Transactions of ASM*, v. 37, p. 27-47, 1946.
15 READY, J.F. LIA Handbook of Laser Materials Processing. Laser Institute of America: Orlando (FL), p. 223-262, 2001.